Single Component Dynamics in Miscible Poly(vinyl methyl ether)/ Polystyrene Blends under Hydrostatic Pressure

Gustavo A. Schwartz,*,†,‡ Juan Colmenero,†,‡ and Ángel Alegría‡

Donostia International Physics Center, Paseo Manuel de Lardizabal 4, 20018 San Sebastián, Spain, and Departamento de Física de Materiales UPV/EHU, Centro de Física de Materiales CSIC-UPV/EHU, Facultad de Química, Apartado 1072, 20080 San Sebastián, Spain

Received November 13, 2006; Revised Manuscript Received February 26, 2007

ABSTRACT: By means of dielectric spectroscopy, we have studied the relaxation dynamics of poly(vinyl methyl ether) (PVME) in miscible blends with polystyrene (PS) at several concentrations in a broad range of pressure and temperature. Several interesting phenomena which take place in these kinds of blends have been investigated. In particular, the validity of the temperature−pressure superposition for a single component in a polymer blend over the whole composition range has been tested. We have also found that isobaric fragility for PVME in the blends increases with pressure whereas it does not change for pure PVME or even decreases for PS. Additionally, the confinement effects on PVME induced by the other component have also been analyzed. Finally, we discuss the ability of the density scaling to account for the low T_g component dynamics in the blend over a broad pressure−temperature range.

1. Introduction

Polymer blends provide a practical an efficient way to fill new requirements for material properties and applications. The physical properties of polymer blends can be continuously varied between those of the pure components without synthesis of new materials. Since the processability of polymer blends (and polymers in general) and the way a glassy material is formed are both related to the molecular motion around T_g, the study of the segmental dynamics is of particular relevance. Besides the technological significance, the dynamics of miscible polymer blends displays peculiar features that make the study of these systems very attractive from a scientific point of view. Among them are the role of self-concentration effects due to chain connectivity,[1,2] the heterogeneous dynamics at the length scale of the segmental relaxation,[3] the broadening of the dynamics relaxation spectrum with blending induced by concentration fluctuations,[4] and the recently reported confinement effects due to the rigidization of the high T_g component.[5−8]

The understanding of the molecular dynamics of the neat polymers, as well as the polymer blends, is hardly possible using temperature as the single thermodynamic variable. By varying temperature, both thermal energy and density change and therefore their specific contribution become indistinguishable. Recent progress in this sense has come from the routine use of pressure as an experimental independent variable,[9−14] and thus, the segmental dynamics has been measured as a function of both pressure and temperature in a wide variety of polymers. In this way the thermal and density contributions to the segmental dynamics can be decoupled. This approach has been successfully applied to pure homopolymers, but very few works have been published for polymer blends.[12,15−19]

The dynamics of PVME has been recently studied under hydrostatic pressure[14] as well as in binary mixtures[20,21] and polymer blends[12,22,23] at atmospheric pressure and also under hydrostatic pressure.[18,24] In this work we will analyze the dielectric dynamics of PVME blended with PS in a broad range of frequency, temperature, and pressure and for the whole composition range. We will focus on how the pressure−temperature behavior of PVME is affected when blended with a second polymer, in this case PS. This system (PVME/PS) is of particular interest because it basically has only one component dielectrically active (the dielectric relaxation strength of PS is much weaker than that of PVME). This fact allows following the dynamics of the PVME in the whole composition range with a reasonable accuracy, which is particularly important for high PS contents. In this last case we can also observe and study how pressure affects the confinement effects on the low T_g component due to the rigid matrix of the high T_g component below a certain temperature. These confinement effects for polymer blends under hydrostatic pressure have been recently reported by Takeno et al.[25] but focusing only on the low-temperature regime. Finally, it is worth noting that we have also analyzed for the first time the dielectric response of pure PS at high pressures.

2. Theoretical Background

Because of the lack of an appropriate framework to fully describe the pressure−temperature dependence of the relaxation times for polymer blends under hydrostatic pressure, we will use in this work two different approaches. On the one hand, we will use a phenomenological description of the relaxation times with the Vogel−Fulcher−Tammann (VFT) equation.[26] On the other hand, we will investigate the applicability of the density scaling to a single component in polymer blends (as well as for the pure polymers). In this section we will briefly summarize the basis of these approaches. For a more detailed explanation the reader is invited to look the references below mentioned. Additionally, we will define here the equilibrium and nonequilibrium dynamics in miscible polymer blends.

Vogel−Fulcher−Tammann (VFT) Equation. The most common way to describe the temperature dependence of the isobaric relaxation times is by means of the phenomenological

* Corresponding author: Tel +34 943 015414; fax +34 943 015600; e-mail schwartz@ehu.es.
† Donostia International Physics Center.
‡ Centro de Física de Materiales CSIC-UPV/EHU.

10.1021/ma062609b CCC: $37.00
Published on Web 03/27/2007

Vogel−Fulcher−Tammann (VFT) equation[26] given by

$$\tau(T) = \tau_0 \exp\left(\frac{DT_0}{T - T_0}\right) \quad (1)$$

where τ_0, D, and T_0 are temperature-independent parameters. Although the VFT equation gives only a phenomenological description of the relaxation times, it is useful to estimate the pressure dependence of characteristic parameters like the dielectric T_g and fragility as described below.

Density Scaling. It has been recently shown[27,28] that for several glass-formers the logarithm of the main (or α-) relaxation time, measured at various temperatures and pressures, yields a master curve when plotted against TV^γ, where γ is a material-specific constant which has been found to vary in the range $0.14 \leq \gamma \leq 8.5$ for the glass-formers investigated to date. The parameter γ provides a measure of the relative importance of V compared to T in the glass-forming dynamics. It is immediately clear that $\gamma = 0$ means a pure thermally controlled dynamics; on the other hand, for the hard spheres limit, $\gamma \rightarrow \infty$ and the dynamics becomes entirely volume dependent. According to Casalini et al.,[27] it is therefore expected that γ correlates with the ratio of the activation enthalpy at constant volume $E_V = R[\partial \log(\tau)/\partial(T^{-1})]_V$ to that at constant pressure $E_P = R[\partial \log(\tau)/\partial(T^{-1})]_P$, E_V/E_P evaluated at T_g.

It is worth noticing that this density scaling law (TV^γ) is not unique, and other density scaling functions were recently proposed.[14] However, other authors[29] claim that some density scaling laws fail for extended ranges of pressure and temperature, although this conclusion was obtained using a significant extrapolation of the *PVT* data which are typically limited to $P \leq 200$ MPa. This controversy is out of the scope of the present work, and therefore the reader is invited to look at refs 14 and 29 for a detailed discussion about different density scaling laws and their limitations.

Equilibrium and Nonequilibrium Dynamics in Miscible Polymer Blends. A very interesting phenomenon in miscible polymer blends with large difference in their T_gs is that the dynamics of the low T_g component can be strongly affected by the slowing down of the dynamics of the high T_g one. At low enough temperatures, or high pressures, the temperature dependence of the relaxation time of the low T_g component, in blends with small low T_g component contents, displays an Arrhenius-type behavior. This kind of behavior was first noticed by Sy and Mijovic[30] and attributed to the ability of the rigid high T_g polymer of the blend to confine the low T_g one. Some authors[31,32] have proposed that this behavior is a sign of an emerging Johari−Goldstein (JG) relaxation, since it has been also observed in other mixtures. This interpretation is not incompatible with the previous one if it is considered that the molecular motions involved in a JG process are of the same nature than those of the segmental dynamics. Nevertheless, along this work we will refer to this behavior as nonequilibrium (or confined) dynamics.

These nonequilibrium effects are particularly important in blends rich in the high T_g component; however, they were also observed, though less pronounced, for other compositions.[5,23] In fact, the effect of the high T_g component on the dynamics of the low T_g one manifests even at higher temperature where the Arrhenius behavior has not appeared yet. In other words, upon temperature reduction the high T_g component dynamics becomes too slow, and the blend as a whole falls out of equilibrium (becoming glassy) whereas the low T_g component dynamics is still experimentally accessible. The pronounced dynamical heterogeneity in the blend component dynamics makes that the nonequilibrium effects starts at a rather ill-defined temperature that can be taken as that of the onset of the DSC glass transition on cooling. Thus, we will define in this work the equilibrium temperature (T_{eq}) as the temperature at which the high T_g component starts becoming frozen and therefore the dynamics of the low T_g component can be affected by nonequilibrium effects. For the low T_g component, the dynamics which takes place above T_{eq} will be called equilibrium dynamics, and that below T_{eq}, nonequilibrium dynamics.

3. Experimental Section

Samples. Blends of poly(vinyl methyl ether) (PVME: $[C_3H_6O]_n$; Aldrich), $M_w = 21\,900$ g/mol ($M_n = 7300$ g/mol), and polystyrene (PS: $[C_8H_8]_n$; Polymer Laboratories), $M_w = 70\,950$ g/mol ($M_n = 66\,900$ g/mol), at three different concentrations were prepared for this study. The pure polymers were dried in a vacuum oven at temperatures above their respective T_g for 48 h. Then, appropriate amounts of each component were dissolved in toluene (5% w/w) and mixed together for 24 h. Because of the brittle character of PS, the method of preparation of the samples for dielectric measurements depends on the PS contents. For low PS contents (25 and 50%) the samples were prepared by putting the solution over a gold-plated electrode, 20 mm diameter, with a spacer of 0.1 mm thickness. The toluene was later evaporated, first at atmospheric conditions for 24 h and later in a vacuum oven, until getting constant weight. Finally, the upper electrode was put over the sample, and the set was slightly pressed, under vacuum and above T_g, to ensure good electrical contact. For higher PS contents very thin disks, 20 mm diameter and 0.1−0.2 mm thickness, were obtained (as previously described) and gold-sputtered on both sides. The diameter of these samples was slightly larger (∼21 mm) than the diameter of the gold-sputtered area on each side (∼19 mm). In this way the conduction path through the oil between both electrodes is significantly larger, and therefore this particular geometry reduces the oil conductivity contribution to the measured losses by, at least, a factor of 10. Blends with 75, 50, and 25 wt % of PVME, namely PVME/PS 75/25, PVME/PS 50/50, PVME/PS 25/75, are analyzed in this work. Additionally, a sample of pure PS was also prepared following the same procedure used for blends with high PS content.

Dielectric Measurements at Atmospheric Pressure. Dielectric measurements were performed using a broadband dielectric spectrometer based on two high-precision dielectric analyzers, one for the frequency range 10^{-2}−10^7 Hz (Alpha analyzer Novocontrol GmbH) and other for the range 10^6−1.8×10^9 Hz (Agilent 4192B), and a Novocontrol Quatro cryosystem for temperature control with a precision better than 0.1 K. Measurements were performed isothermally over a broad frequency and temperature range, starting from high temperatures and with temperature steps of typically 5 K.

Dielectric Measurements under Pressure. Dielectric measurements were carried out in a pressure cell (0−300 MPa) supplied by Novocontrol GmbH. The cell, basically a stainless steel cylinder with a hermetic seal, is filled with a silicone fluid which transmits the pressure from the piston to the sample. The dielectric loss was measured in the frequency range 10^{-2}−10^6 Hz, with a broadband Alpha dielectric analyzer (Novocontrol GmbH). The measurements were performed by frequency sweeps at constant temperature, after stabilizing the temperature of the cell for about 2 h, with stability better than ±0.1 K, and constant pressure, with stability better than ±2 MPa. After each frequency sweep the pressure was changed, at constant temperature, to the next value, and once the highest pressure data were measured, the pressure was reduced to the atmospheric value and the temperature was changed. The measurements have shown a very good reproducibility after repeating them several times.

4. Results

Pure PS. The dielectric response of pure PS under hydrostatic pressure has not been reported until now to the best of our

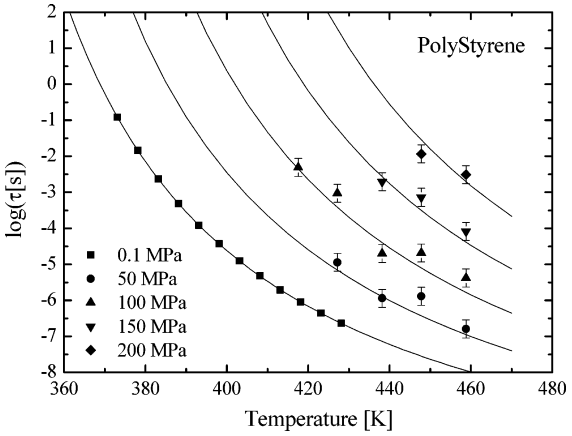

Figure 1. Segmental relaxation time of PS as a function of the temperature at different pressures (from bottom to top: $P_{atm} = 0.1$, 50, 100, 150, and 200 MPa). The lines represent the best fit of the experimental data by means of eq 3 (see text).

knowledge. Besides the very low dielectric signal of the α-relaxation, which is actually not a problem with the available analyzers, the brittle character of PS causes difficulties when a pressurized-liquid based system is used to measure the dielectric response under hydrostatic pressure because the conductivity of the pressurized liquid can screen the weak dielectric signal of PS. In order to minimize the effect of the liquid's conductivity, the sample was gold-sputtered on both sides and a particular geometry was used as previously described. The spectra were described using the Havriliak−Negami (HN) function

$$\epsilon^*(\omega) - \epsilon_\infty = \frac{\Delta\epsilon}{[1 + (i\omega\tau_{HN})^\alpha]^\beta} \qquad (2)$$

where $\Delta\epsilon$ is the relaxation strength, τ_{HN} is a relaxation time, and α and β are shape parameters. An additional term for the conductivity contribution ($-i\sigma_0/\epsilon_0\omega^s$) has been added for the fitting procedure. ϵ_0 is the dielectric permittivity of vacuum, s is a constant factor ($0 < s \leq 1$), and σ_0 is the dc conductivity when $s = 1$. For purposes of this work, the characteristic relaxation time will be that of maximal loss $\tau_{max} = \omega_{max}^{-1} = 1/(2\pi f_{max})$.

Figure 1 shows the temperature dependence of the maximum relaxation time, τ_{max}, of the α-relaxation for pure PS at several pressures. As shown in this figure, just a few points could be measured at high pressures due to the experimental difficulties previously mentioned. The lack of enough experimental points makes difficult, or even impossible, to use the VFT equation at each individual pressure. Instead, we first fitted the data at atmospheric pressure with all the variables as free parameters, obtaining an excellent fit of the experimental data, as shown in Figure 1, with $\log(\tau_0) = -12.87 \pm 0.03$, $D = 5.27 \pm 0.05$, and $T_0 = 313.2 \pm 0.3$ K. Among the several "natural" extensions of the VFT equation[33−35] to describe the pressure−temperature dependence of the relaxation times, we used a simple and natural extension which assumes a linear pressure dependence for the parameters D and T_0. Thus, for the higher pressures we can fit the whole set of experimental data with the following equation

$$\tau = \tau_0 \exp\left\{\frac{(D + m_D P)(T_0 + m_T P)}{T - (T_0 + m_T P)}\right\} \qquad (3)$$

which has only two adjustable parameters (m_D and m_T) after fixing τ_0, D, and T_0 to the values calculated at atmospheric pressure. Note that for $P = 0$ the standard VFT equation is

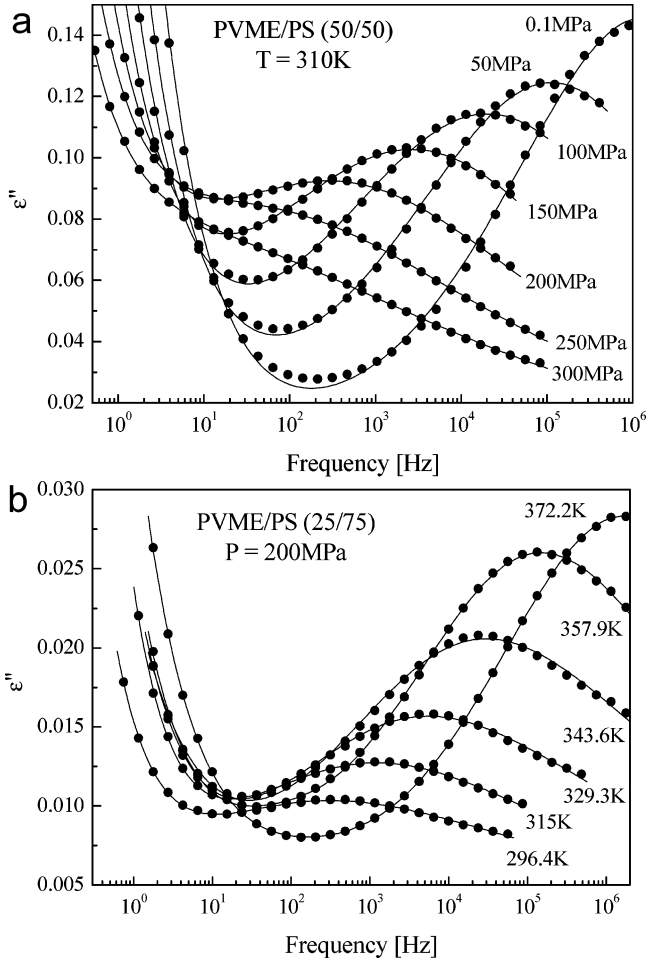

Figure 2. (a) Dielectric loss (ϵ'') as a function of the frequency for PVME/PS (50/50) at constant temperature and different pressures (from left to right: 300, 250, 200, 150, 100, 50, and 0.1 MPa). (b) Dielectric loss (ϵ'') vs frequency for PVME/PS (25/75) at constant pressure and different temperatures (from left to right: 296.4, 315, 329.3, 343.6, 357.9, and 372.2 K).

recovered. We calculated the pair m_D and m_T which minimizes the mean-square deviation between the experimental data and the relaxation times given by eq 3, obtaining $m_D = (9.5 \pm 0.1) \times 10^{-3}$ MPa^{-1} and $m_T = 0.19 \pm 0.01$ K MPa^{-1}. Solid lines in Figure 1 represent the relaxation times predicted by eq 3 with the so-calculated parameters. We will discuss in the next section the plausibility of this approach.

Polymer Blends. Parts a and b of Figure 2 show representative dielectric loss (ϵ'') as a function of the frequency for PVME/PS blends with a composition of 50/50 and 25/75, respectively. Figure 2a shows spectra at constant temperature and different pressures, whereas Figure 2b shows isobaric spectra at several temperatures. Spectra at different pressures (and constant T) look like those measured at different temperatures (and constant P) at the same relaxation time, after normalizing the dielectric relaxation strength. This temperature−pressure superposition is shown in Figure 3a−c, where spectra measured at very different pressures and temperatures show a perfect overlapping within the experimental uncertainties, for each of the three here studied compositions. We chose three different representative conditions to illustrate the $P-T$ superposition. Figure 3a shows equilibrium data, i.e., well above blend's T_g, for three different spectra of PVME/PS 75/25 blend. Figure 3b shows the $P-T$ superposition for data corresponding to the 50/50 blend, for pressures and temperatures where the onset of the nonequilibrium effects could be expected. Finally, in Figure 3c we can observe the excellent

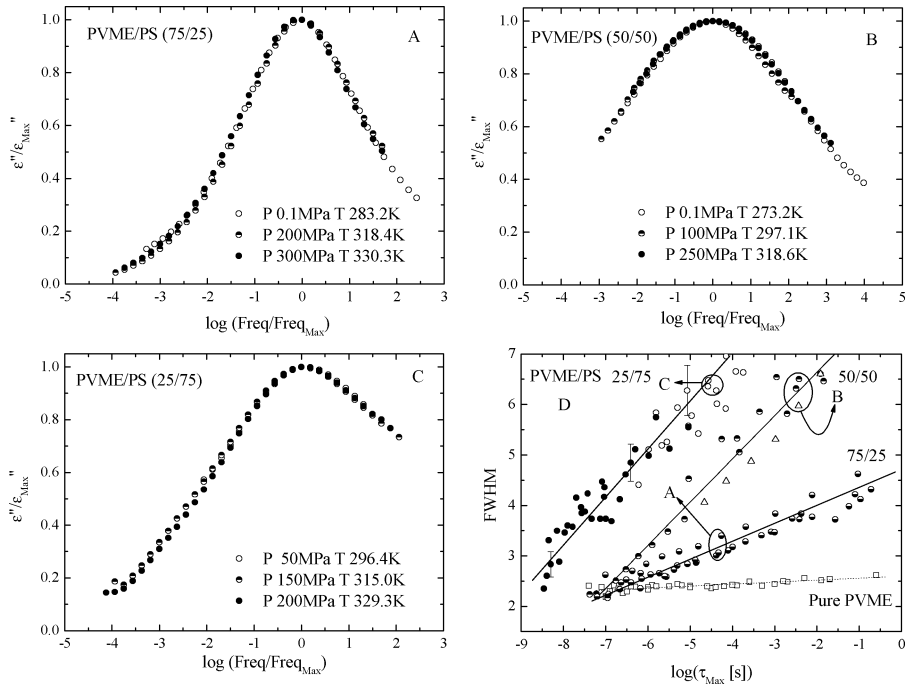

Figure 3. (A−C) Overlapping of different spectra at the indicated conditions for 75/25, 50/50, and 25/75 composition blends. (D) Full width at half-maximum (fwhm) vs logarithm of the maximum relaxation time ($\log(\tau_{max})$), at several pressures and temperatures, for PVME both pure and blended with PS at different concentrations. Open squares represent the experimental data for pure PVME.[14] Lower and upper half filled circles represent the corresponding data for 75/25 and 50/50 compositions, respectively. Open triangles represent out-of-equilibrium data for the 50/50 blend. Filled and open circles represent equilibrium and confined data for 25/75 composition (see text). Vertical error bars represent typical error in the determination of fwhm. The lines are guides to the eye.

overlapping of three different spectra for out of equilibrium data from the PVME/PS 25/75 blend. In the three cases we selected spectra with similar relaxation times and the maximum difference in pressure. In these figures both axis were normalized to remove small differences in the relaxation times and/or relaxation strength. This temperature−pressure superposition has been shown in previous works[14,36,37] for homopolymers; however, little attention has been paid to this superposition for a single component in polymer blends.[12,18]

A different way to show this $P-T$ superposition is to represent the full width at half-maximum (fwhm) of each spectrum against the logarithm of its maximum relaxation time. This is particularly useful when the number of pressures, temperatures, and compositions is rather large, like in the present work. Additionally, this particular representation also shows the correlation between these two variables (fwhm and $\log(\tau_{max})$). Thus, Figure 3d shows the fwhm of the α-relaxation of the PVME as a function of the corresponding maximum relaxation time for all the here studied blend compositions at different temperatures and pressures. For those spectra which are mainly within the experimental frequency window, the value of the fwhm was determined from the shape parameters of the HN equation (α and β) by means of the following empirical equation (see the Appendix):

$$\mathrm{fwhm}(\alpha,\beta) = -0.516 + \frac{1.058}{\alpha} + \frac{0.039}{\beta} + \frac{0.563}{\alpha\beta}$$

Open squares in Figure 3d represent the experimental data for pure PVME taken from ref 14. For pure PVME the fwhm is just slightly dependent on the logarithm of the relaxation time. On the contrary, for the PVME in the blends a much stronger dependence is observed, as shown in Figure 3d. The higher scattering of the data for PVME in the blends is due to the fact that both the dipole dilution and the broadening of the peaks make more difficult the accurate determination of fwhm.

The most interesting fact depicted in Figure 3 is that the temperature−pressure superposition applies not only for pure PVME (which is in agreement with what is often observed in other polymers[14]) but, more interestingly, also for the dynamics of PVME blended with PS over the whole concentration range, including the poor PVME side where the confinement effects are very pronounced (see discussion below). The fact that for each composition all the points, obtained at different temperatures and pressures, collapse around a single line (within the experimental uncertainties) implies that accounting for the temperature−pressure effects on the relaxation time allows predicting the shape of the loss peak once it is measured at atmospheric pressure. Thus, we will turn now to the analysis of the relaxation times, where we will first use a phenomenological approach by means of the VFT equation (eq 1).

PVME/PS (75/25). Figure 4 shows the maximum relaxation times for PVME in PS (75/25) as a function of the temperature at different pressures. Solid lines in Figure 4 represent the best fits to the experimental data through eq 1. The experimental data at atmospheric pressure were first fitted by leaving $\log(\tau_0)$, D, and T_0 as free parameters. We obtained $\log(\tau_0\ [\mathrm{s}]) = -12.3 \pm 0.1$, $D = 6.2 \pm 0.1$, and $T_0 = 212.1 \pm 0.2$ K. Then, $\log(\tau_0)$ was fixed (at the value found at atmospheric pressure) for higher pressures, leaving only D and T_0 as free parameters. The corresponding parameters so obtained are listed in Table 1. We can observe in Figure 4 that the VFT equation fits the experimental points in the whole range of temperatures and pressures. Note that D parameter results essentially pressure independent, whereas T_0 monotonically increases with pressure.

PVME/PS (50/50). Figure 5 shows the maximum relaxation times for PVME in this blend as a function of the temperature at different pressures. Although the nonequilibrium effects in the dynamics are not evident from the relaxation map, we know from previous results[23] that the equilibrium temperature (T_{eq}) for PVME in this blend is about 300 K, and therefore the

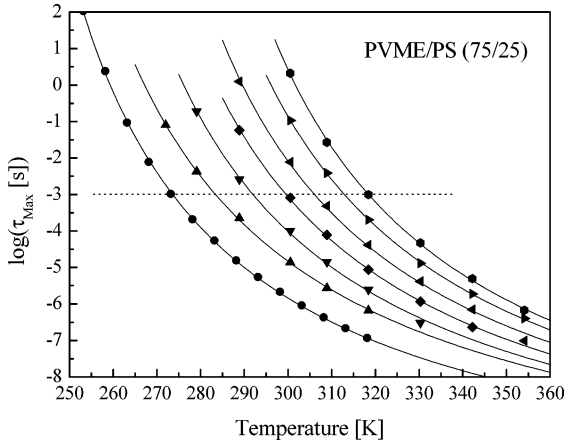

Figure 4. Logarithm of the relaxation time vs temperature at different pressures (from bottom to top: $P_{atm} = 0.1$, 50, 100, 150, 200, 250, and 300 MPa) for PVME in PS (75/25). Solid lines represent the best fit of the experimental data through eq 1. The horizontal dotted line represents the time at which T_g and fragility (m) are defined in this work (see text).

equilibrium dynamics takes place above this temperature (at atmospheric pressure). Consequently, we used for the fitting procedure only those experimental data within the equilibrium dynamics range. The fitting procedure was performed as in the previous case, by leaving $\log(\tau_0)$, D, and T_0 as free parameters at atmospheric pressure. We obtained $\log(\tau_0\ [s]) = -12.3 \pm 0.2$, $D = 5.9 \pm 0.1$, and $T_0 = 220 \pm 1$ K. Then $\log(\tau_0)$ was fixed to the value so obtained (at atmospheric pressure), and only D and T_0 were left as free parameters for the higher pressures. The corresponding parameters are listed in Table 1. Solid lines in Figure 5 represent the best fits to the experimental data through eq 1. The fitting is again excellent as shown in Figure 5. As shown in Table 1, a slight but monotonic increment of the fragility for PVME (decrement of D parameter) with pressure is found at this concentration.

PVME/PS (25/75). Figure 6 shows the maximum relaxation times for PVME in PS (25/75) as a function of the inverse temperature at different pressures. The confinement effects are clearly evident for this composition. The experimental points at each pressure clearly depart from the high-temperature VFT behavior and gradually go toward an Arrhenius one upon temperature reduction. The dotted diagonal line in Figure 6 indicates, approximately, the temperature range at which PVME dynamics seems to depart from the VFT-like behavior. As mentioned in the Introduction, this behavior has been related to the fact that below the blend's T_g the system goes out of equilibrium, and the low T_g component becomes confined by the rigid matrix formed by the high T_g component.[5−8]

Since there are few experimental points (at each pressure) within the equilibrium window, the use of the VFT equation at each individual pressure makes the fitting procedure unstable. Instead, we used to fit these data the same procedure followed above for pure PS. This procedure is additionally supported by the fact that for the other blends $D(P)$ and $T_0(P)$ approximately follow linear laws. For the atmospheric pressure data we knew from a previous work[23] that PVME deviates from equilibrium dynamics at around 325 K; accordingly, we first fitted, with the VFT equation, the atmospheric data above this temperature. We obtained $\log(\tau_0\ [s]) = -12.1 \pm 0.3$, $D = 5.5 \pm 0.2$, and $T_0 = 225 \pm 2$ K. Then, for the data at higher pressures (and within the equilibrium window), we kept constant the value of τ_0 and assumed a linear pressure dependence for parameters D and T_0; i.e., we use eq 3 to fit the whole set of experimental data at this concentration. As before, we have only two fitting parameters (m_D and m_T) after fixing τ_0, D, and T_0 to the values calculated at atmospheric pressure. Solid curved lines in Figure 6 represent the best fit of the equilibrium experimental data through eq 3 with $m_D = (-6.0 \pm 0.5) \times 10^{-3}$ MPa^{-1} and $m_T = 0.21 \pm 0.01$ K MPa^{-1}. The so-obtained VFT parameters are listed in Table 1. As in the previous case, an increase of the fragility (decrement of D parameter) with pressure is also found at this concentration.

The behavior at each pressure for temperatures below the crossover range was fitted with an Arrhenius law ($\tau = \tau_0 \exp(E/RT)$), as shown in Figure 6. The resulting parameters are listed in Table 2. The activation energy slightly decreases with pressure whereas $\log(\tau_0)$ does vary with pressure, indicating a retardation of the relaxation times with increasing pressure. These results are in a good agreement with those recently found by Takeno et al.[25] for a similar composition (PVME/PS (20/80)). A more detailed discussion will be given in the next section.

5. Discussion

Fwhm. The pressure−temperature superposition, previously reported for pure polymers, has been found to be also valid for the single component dynamics in a polymer blend over the whole composition range, as shown in Figure 3a−c. This behavior is in agreement with previous observations[12,18] on the PVME-rich side. However, it is remarkable the fact that the pressure−temperature superposition is still valid for out of equilibrium data. Figure 3c shows the perfect overlapping of three different spectra for the 25/75 blend, where at low temperatures and/or high pressures the dielectric relaxation is due to the dynamics of confined PVME in the PS matrix (see open circles in Figure 3d). Moreover, as shown in Figure 3b, the $P-T$ superposition is still valid when applied over the temperature range where the onset of nonequilibrium effects is expected.

Although the pressure−temperature superposition works rather well for the 25/75 blend, a significant difference appears between the results for this blend and those for the blends 50/50 and 75/25, as shown in Figure 3d. For the PVME richer blends the fwhm values tend toward the behavior of the pure polymer at relaxation times of about 10^{-7} s (see Figure 3d), whereas for the blend 25/75 the pure PVME fwhm values would meet for much shorter relaxation times, of about 10^{-9} s. This means that in order to recover the pure PVME $\log(\tau_{max})$ dependence of fwhm for this latter blend, one needs to access very short times, where the intrachain motions would dominate the observed dynamics. This is not the case for the PVME-rich blends for which the pure PVME fwhm values would be recovered once the relevant volume around a PVME unit becomes small enough to include only other PVME segments.

All these new results are worth to be deeply studied in future works by means of high-frequency techniques (microwave dielectric relaxation or neutron scattering). Work in this direction is in progress.

Pure Polymers Dynamics. We will discuss now the behavior of the pure polymers. As mentioned before, the dielectric response of PS at high pressures is here presented for the first time, and therefore we cannot compare our results with other previously published. However, it is possible from our results to get the pressure dependence of the dielectric T_g (i.e., $T(\tau = 10^2$ s)) and the isobaric fragility (m) which have been previously measured by other methods. The isobaric fragility (m) is usually defined as the slope of the curve $\log(\tau_{max})$ vs T_g/T at $T = T_g$, i.e., $m = \mathrm{d}\log(\tau)/\mathrm{d}(T_g/T)|_{T=T_g}$. From Figure 1 and eq 3 we can

Table 1. VFT Parameters for PVME in PS at the Indicated Concentrations[a]

	PVME/PS 75/25		PVME/PS 50/50		PVME/PS 25/75	
P [MPa]	D	T_0 [K]	D	T_0 [K]	D	T_0 [K]
0.1	6.2 ± 0.1	212.1 ± 0.2	5.9 ± 0.1	220 ± 1	5.5 ± 0.2	225 ± 2
50	6.7 ± 0.1	215.9 ± 0.4	5.4 ± 0.2	234 ± 2	5.2 ± 0.2	236 ± 2
100	6.2 ± 0.1	226.2 ± 1.0	5.5 ± 0.5	239 ± 5	4.9 ± 0.2	246 ± 2
150	6.1 ± 0.1	232.9 ± 0.5	4.9 ± 0.2	251 ± 2	4.6 ± 0.2	257 ± 2
200	6.2 ± 0.1	237.8 ± 1.0	4.4 ± 0.2	263 ± 2	4.3 ± 0.3	267 ± 3
250	6.2 ± 0.1	243.0 ± 0.5	4.6 ± 0.2	264 ± 2	4.0 ± 0.3	278 ± 3
300	6.0 ± 0.1	249.3 ± 0.7	4.1 ± 0.2	274 ± 2	3.7 ± 0.3	288 ± 3

[a] See text for details about the fitting procedure.

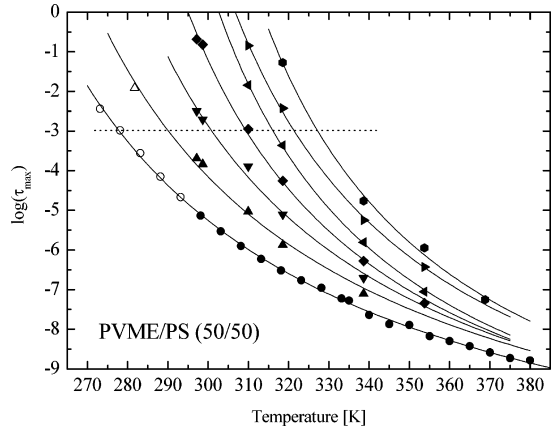

Figure 5. Logarithm of the relaxation time vs temperature at different pressures (from bottom to top: $P_{atm} = 0.1$, 50, 100, 150, 200, 250, and 300 MPa) for PVME in PS (50/50). Solid lines represent the best fit of the experimental data through eq 1. Open symbols refer to experimental data where the system is out of equilibrium. The horizontal dotted line is defined as in Figure 4.

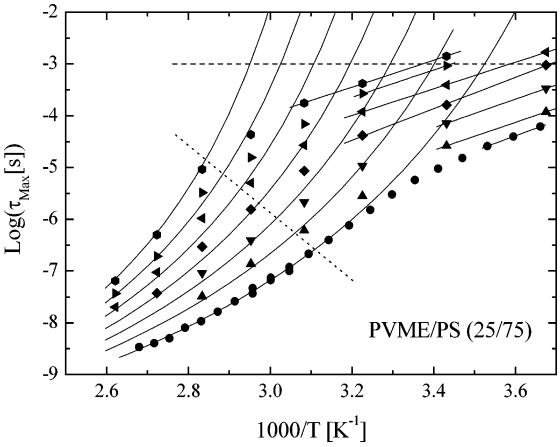

Figure 6. Logarithm of the relaxation time vs inverse temperature at different pressures (from bottom to top: $P_{atm} = 0.1$, 50, 100, 150, 200, 250, and 300 MPa) for PVME in PS (25/75). Solid curved lines represent the best fit of the experimental data through eq 1. The dotted diagonal line refers to the temperature range below which the high T_g component is out of equilibrium, and therefore confinement effects start appearing. Straight solid lines represent the Arrhenius fit for the out-of-equilibrium data at each pressure (see text). The horizontal dotted line is defined as in Figure 4.

calculate the dielectric T_g and m as a function of the pressure; the results are shown in Figure 7. We found that the pressure dependence of the dielectric T_g for PS is $dT_g/dP = 320 \pm 24$ K/GPa, well within the range of previously calculated values by other techniques[29] (360 and 303 K/GPa by means of PVT and DTA measurements, respectively). On the other hand, the isobaric fragility obtained at atmospheric pressure ($m = 112 \pm 5$) is, within experimental errors, equal to the previously published value of 116.[38] Concerning the pressure dependence

Table 2. Arrhenius Parameters for PVME in PS (25/75) at Temperatures below Its Effective T_g[a]

P [MPa]	$\log(\tau_0$ [s])	E [kJ/mol]	P [MPa]	$\log(\tau_0$ [s])	E [kJ/mol]
0.1	-14.9 ± 0.5	57.7 ± 1.9	200	-12.2 ± 0.5	51.0 ± 1.5
50	-13.8 ± 0.6	53.4 ± 1.8	250	-12.1 ± 0.6	52.4 ± 2.0
100	-13.6 ± 0.4	54.8 ± 1.9	300	-11.7 ± 0.5	51.4 ± 1.7
150	-14.2 ± 1.2	60.1 ± 2.4			

[a] See text for details about the fitting procedure.

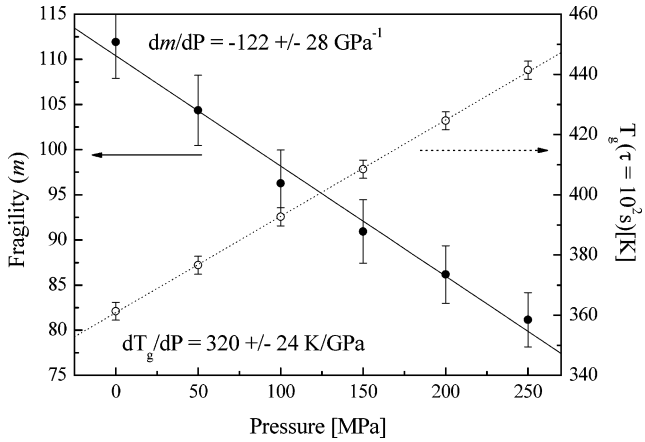

Figure 7. Fragility (m) (filled circles) and dielectric T_g (open circles) as a function of the pressure for pure PS. The lines represent the best linear fits to the experimental data. The slopes of these lines are shown in the figure as dm/dP and dT_g/dP, respectively.

of the isobaric fragility, this value is rather dependent on the pressure interval. For the whole pressure range we got $dm/dP = -122 \pm 28$ GPa^{-1}, which is slightly different than that one (-160 GPa^{-1}) calculated by Huang et al.[39] from photon correlation data. However, if we restrict the pressure range to that of the photon correlation data used by Huang et al., we get $dm/dP = -157$ GPa^{-1}. This good agreement between our results and those previously published supports the validity of our analysis of the pressure-temperature dependence of the relaxation times for pure PS by means of the VFT equation as previously described.

A different way to present the dielectric relaxation time measured at various pressures and temperatures is by using a density scaling function ($X(V,T)$). If this density scaling works, then, by plotting the maximum relaxation time against X, the experimental data points measured at different pressures and temperatures will collapse into a single curve. Although the most common used density scaling function is $X = TV^{\gamma}$, it is worth noticing here that this is not unique as was shown in previous works;[14,28] however, the validity of other density scaling laws for extended ranges of pressure and temperature is still under debate.[14,29] Figure 8 shows the maximum relaxation time for PS measured at different pressures and temperatures, as a function of TV^{γ}, where V represents the specific volume

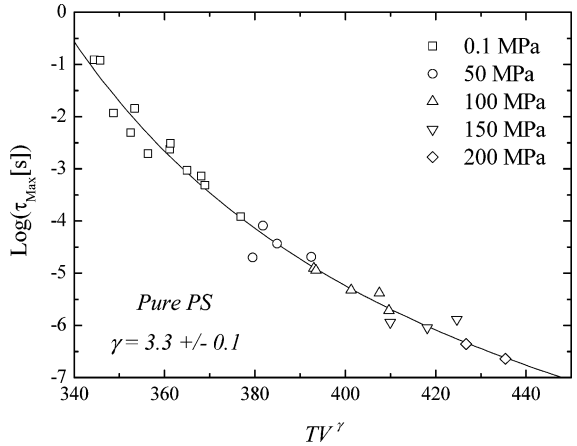

Figure 8. Maximum relaxation time of pure PS, measured at different temperatures and pressures, as a function of TV^{γ}. The symbols represent the same values of pressures than in Figure 1. The value of the γ parameter is shown in the figure. The line represents the best fit of the experimental data with an empirical VFT-like equation (see text).

expressed in cm^3/g. The parameter γ was adjusted to yield a master curve with a minimum mean-square deviation; the so-obtained value is $\gamma = 3.3 \pm 0.1$. The experimental data in Figure 8 are more scattered than for other polymers[14] because of the experimental difficulties to measured PS, as previously commented on; nevertheless, the value of γ is within the expected ones for polymeric systems according to previous results.[14,27] In particular, for pure PVME it was found $\gamma = 2.5 \pm 0.05$.[14,29]

We have shown in a previous work[14] that once the density scaling is performed, the so-obtained master curve can be well fitted with an empirical VFT-like equation given by

$$\tau(X) = \tau_0 \exp\left(\frac{D_X X_0}{X - X_0}\right) \tag{4}$$

where $X = TV^{\gamma}$, $X_0 = T_0 V_0^{\gamma}$, and τ_0 is fixed to the relaxation time at high temperatures obtained from eq 1 at atmospheric pressure. The parameter D_X is related with a generalized fragility m_x, defined following ref 28 as the steepness of the $\log(\tau)$ vs X_g/X at X_g, through $m_x = \mathrm{d}\log(\tau)/\mathrm{d}(X_g/X)|_{x=x_g}$. It is clear from eq 4 that for $\gamma = 0$, i.e., a fully temperature-controlled process, the standard VFT equation is recovered. The solid line in Figure 8 represents the best fit of the experimental data with eq 4, with $\log(\tau_0) = -12.87$, $D_X = 11.0 \pm 4.2$, and $X_0 = 244 \pm 19$ K. An important consequence of eq 4 is that according to previous results[14] the parameter D_X seems to be independent of the density scaling function $X(V,T)$ used to superimpose the experimental data, and hence it would be an intrinsic characteristic of each material.

Polymer Blends Dynamics. Turning to the dynamics of PVME, an interesting aspect to analyze is how its fragility is affected by blending it with a second polymer. We have already mentioned that the isobaric fragility (m) is usually defined as the slope of the curve $\log(\tau)$ vs T_g/T at $T = T_g$. However, the relaxation times of our experimental data points within the "equilibrium window" are far from 100 s, especially for the PVME/PS (25/75). Thus, to avoid an excessive extrapolation of the experimental relaxation times to 100 s, we will define for the purpose of the comparison between the different samples in this work, a fragility at an intermediate relaxation time of 10^{-3} s. Thus, we have $m^* = \mathrm{d}\log(\tau)/\mathrm{d}(T_g^*/T)|_{\tau=10^{-3}\mathrm{s}}$, where $T_g^* = T(\tau = 10^{-3}\ \mathrm{s})$ is calculated from the VFT lines describing the equilibrium dynamics in the dielectric relaxation map. The horizontal dashed lines in Figures 4−6 indicate the relaxation time at which T_g^* and m^* were calculated. Table 3 shows the obtained values of T_g^* and m^* for pure PVME and PS and for the PVME in the blends at the different compositions. The dielectric T_g^* so obtained increases with pressure, as expected. However, the fragility (m^*) of PVME in the blends presents more surprising results. Whereas the value of m^* obtained for pure components keeps constant (PVME) or decreases with increasing pressure (PS), m^* increases with pressure for blends with 50 and 25% of PVME. Astonishingly, the higher the PS content the higher the increment of m^* with pressure. Even more interesting is the fact that for most glass-formers the fragility decreases with pressure,[29] whereas we observe that for PVME in blends with PS the fragility presents the opposite behavior, increasing with pressure. Whether this finding is a general trend for the component dynamics in polymers blends or this is an isolated anomalous behavior is something which definitely needs further investigations.

Other interesting feature to be considered is the influence of pressure on the confinement effects that takes place in polymer blends under certain conditions. As aforementioned, when two polymers with very different T_g values are blended, there is a temperature range around the blend's T_g, where for the low T_g component a continuous departure of the experimental relaxation times from the high-temperature VFT behavior (toward an Arrhenius one) is observed, as clearly shown in Figure 6. These confinement effects in PVME/PS blends at atmospheric pressure have been analyzed by us in recent works;[5,23] above atmospheric pressure, Takeno et al.[25] have recently reported these effects on the same blend but mainly focused on the low-temperature range. We analyze here the full temperature−pressure interval for the whole composition range, i.e., both equilibrium- and confinement-controlled behaviors.

From our previous experience,[5,23] we expected that the temperature where the confinement effects start appearing increases with decreasing PVME content. Thus, the effects of the high T_g component on the low T_g one should be much more remarkable in the PVME/PS (25/75) blend. Actually, Figure 6 shows how the experimental relaxation times depart from the (high temperature) VFT behavior upon temperature reduction at temperature values (T_{eq}) which change with pressure, as approximately indicated by the diagonal dashed line in the figure. The relaxation times become faster than expected for temperatures below T_{eq}. A possible explanation for this behavior is that the cooperativity in the low T_g component is limited by the rigid matrix of the high T_g component. Thus, the low T_g component is confined by the glassy matrix of the second polymer limiting the cooperativity extent of the relaxation processes. Once the cooperativity is restricted, only the more local relaxation processes can be realized, being faster than the cooperative ones that would occur at equilibrium at the same temperature. Because large cooperative rearrangements become forbidden, the dipole reorientations are restricted, and there is a consequent reduction of the relaxation strength (see low-temperature data in Figure 2b). This interpretation is in agreement with that of Takeno et al.[25] At temperatures well below the blend's T_g the relaxation times follow an Arrhenius behavior, as indicated by the straight lines in Figure 6, with the corresponding parameters listed in Table 2. From these values we observe that the activation energy just slightly decreases with pressure, which indicates that the underlying mechanism does not strongly depend on pressure. On the other hand, $\log(\tau_0)$ significantly varies with pressure, turning the process slower and slower with increasing pressure.

Table 3. Dielectric $T_g^*(\tau = 10^{-3}$ s) and m^* ($\tau = 10^{-3}$ s) for Pure PVME and PS and the Different Concentrations (Errors Are ±1 of the Least Significant Digit)

P [MPa]	pure PVME	PVME/PS (75/25)	PVME/PS (50/50)	PVME/PS (25/75)	pure PS
			$T_g^*(\tau = 10^{-3}$ s) [K]		
0.1	265	274	281	284	386
50	274	283	293	294	404
100	281	292	300	304	423
150	289	299	308	313	442
200	296	307	317	322	462
250	303	313	321	330	
300	310	319	326	339	
			m^* ($\tau = 10^{-3}$ s)		
0.1	41	41	43	44	52
50	41	39	46	46	49
100	41	41	45	48	46
150	41	42	50	51	43
200	41	41	55	53	41
250	41	41	53	57	
300	41	42	58	61	

Finally, we will analyze the ability of the density scaling to give account for the component dynamics in the here investigated polymer blends. To perform any density scaling, we need to know the equation of state for the blends at the different compositions. Since the blend PVME/PS has been widely studied, we took *PVT* data from the literature; we used the Tait[40] equation with the parameters given in ref 17 for concentrations of 50 and 70% of PVME. For PVME/PS 25/75 blend the PVT data were taken from ref 41. Parts a and b of Figure 9 show the density scaling for the blends with 75 and 50% PVME, respectively. For the highest PVME content, namely PVME/PS (75/25), the density scaling works well with $\gamma = 1.85 \pm 0.05$. This value of γ is lower than that of the pure PVME ($\gamma = 2.5$) and different from that previously calculated by Roland and Casalini in ref 17. In that reference the authors used a narrower range of pressures and temperatures obtaining for the density scaling $\gamma = 3$; if we restrict the temperature−pressure range of the data under consideration to that used in ref 17, we observe that the density scaling still works but with $\gamma = 2.0$, as shown in the inset of Figure 9a. For PVME in the PVME/PS (50/50) blend the master curve obtained after applying the density scaling does not show a good overlapping, and a relatively big dispersion is observed for the best case ($\gamma = 2.25$), as shown in Figure 9b. Moreover, a systematic change of the curvature with pressure is observed for this composition, indicating that the dispersion is not due to experimental uncertainties but due to a failure of the density scaling procedure (see Figure 9b). These results are in apparent contradiction with that obtained by Roland and Casalini[17] (good overlapping with $\gamma = 3$) on the same blend, although with different PVME molecular weight. The difference between our results and those published in ref 17 could be due to this difference in PVME molecular weight (21 900 g/mol in this work and 99 000 g/mol in ref 17). Although the difference in molecular weight (for this M_w range) does not affect the PVT response, it could affect the thermodynamics of the blends and consequently the magnitude of the concentration fluctuations. This would manifest on the dielectric relaxation results as different values of the maximum and mean relaxation times, which could be at the origin of the differences between our results and those appearing in ref 17. If we again restrict the temperature−pressure range of our data to that used in ref 17, a relatively good overlapping of the experimental points for the 50/50 blend is obtained with $\gamma = 3$, as shown in the inset of Figure 9b. This means that for a broader range of temperatures and pressures the density scaling in the present form does not work as well as for pure polymers, at least for the dependence of the maximum relaxation time here analyzed. We also observe a failure of the density scaling procedure for the PS richest blend, i.e., PVME/PS 25/75. We can observe from Figure 6 that the "equilibrium window", where it is possible to apply the density scaling, is very small (about 2 orders of magnitude for the relaxation times). Even for this

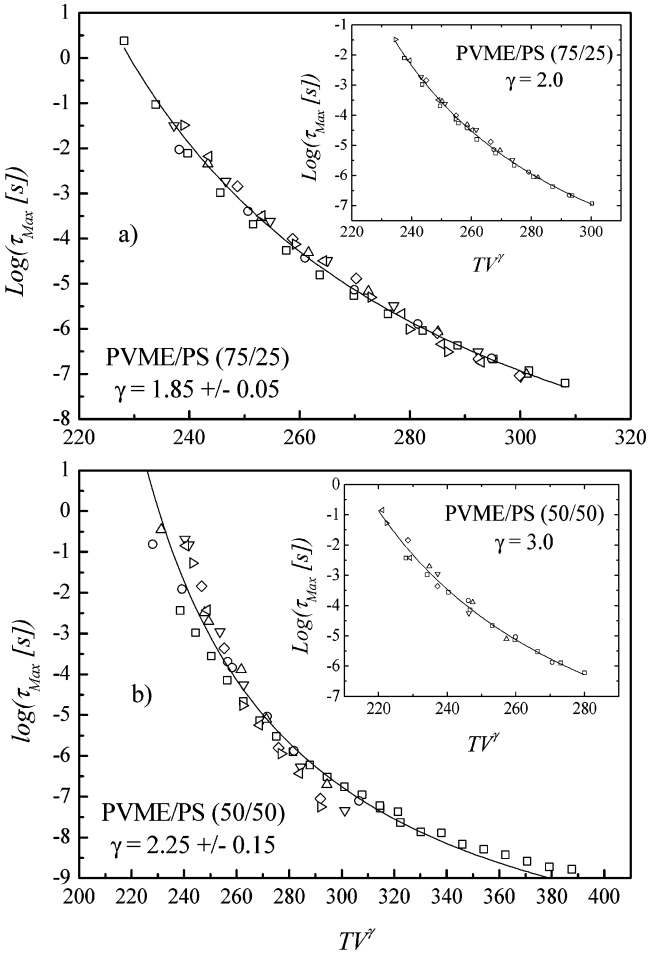

Figure 9. Maximum relaxation time of PVME in (a) PVME/PS (75/25) and (b) PVME/PS (50/50), measured at different temperatures and pressures, as a function of TV^γ. Squares represent data at 0.1 MPa, circles 50 MPa, up triangles 100 MPa, down triangles 150 MPa, diamonds 200 MPa, left triangles 250 MPa, and right triangles 300 MPa. The value of γ for each concentration is shown in the figure. The insets represent the maximum relaxation time of PVME in (a) PVME/PS (75/25) and (b) PVME/PS (50/50), as a function of TV^γ for the same temperature−pressure range than in ref 17. The lines are guides to the eye.

small range, the best temperature−pressure superposition (not shown) shows a systematic increment of the curvature with increasing pressure.

It is noteworthy that a conceptual problem arises with the density scaling applied to a single component in a polymer blend: what volume should be used? First, the dynamics followed by dielectric spectroscopy is not the average dynamics but that of a single component. Thus, because of the presence of fluctuations of concentration, the dynamics in rich PVME regions is highlighted. In addition, at a given temperature the compressibility of PVME is always greater than that corresponding to PS, and therefore the effective local volume around a PVME monomer at a given pressure and temperature will be likely smaller than that assumed from the *PVT* data of the whole sample. Thus, it is not clear that the macroscopic volume of the whole sample, as measured by *PVT*, reflects what really happens at the length scale of the segmental relaxation of the observed component. These considerations should be taken into account when applying the density scaling to a single component in a polymer blend and therefore put into question the previous results.

6. Conclusions

We have analyzed in this work the component dynamics in a miscible polymer blend (PVME/PS) at different concentrations under a broad range of frequency, temperature, and pressure. The validity of the pressure−temperature superposition for a single component in a miscible polymer blend over the whole composition range has been shown; moreover, the superposition is still valid for the low T_g component even when it is confined by the other component. We have seen that the single component fragility is strongly affected by blending, giving a pressure dependence opposite to that of the pure components. This is a new result which is worth to be deeply investigated in further works. Finally, the ability of the density scaling to account for the dynamics of the low T_g component in PVME/PS 50/50 and 25/75 blends for the range of pressures and temperatures explored in this work has been put into question. It is also noticeable that we have reported and analyzed for the first time the dielectric response of pure PS under hydrostatic pressure.

Acknowledgment. This work has been supported in part by the Spanish Ministry of Science and Technology (MICyT) (project MAT 2004/01617) and by the Government of the Basque Country (project 9/UPV 00206.215-13568/2001). The authors also thank the support of the SoftComp NoE/NMP3-CT-2004-502235.

Appendix

In this Appendix we will show the numerical method developed to determine the fwhm (full width at half-maximum) of the loss peak from the shape parameters (α and β) of the Havriliak−Negami (HN) equation. The HN equation can be written as

$$\epsilon^*(\omega) - \epsilon_\infty = \frac{\Delta\epsilon}{[1 + (i\omega\tau_{HN})^\alpha]^\beta} \qquad (A.1)$$

where $\Delta\epsilon$ is the relaxation strength, τ_{HN} is a relaxation time, and α and β are shape parameters. Since fwhm only depends on α and β, $\Delta\epsilon$ and τ_{HN} will be set to one and ϵ_∞ to zero for simplicity. On the other hand, we know from ref 24 that

$$\tau_{max} = \sin\left(\frac{\alpha\pi}{2+2\beta}\right)^{-1/\beta} \sin\left(\frac{\alpha\beta\pi}{2+2\beta}\right)^{1/\beta} \qquad (A.2)$$

And once the height at τ_{max} is determined, by replacing (A.2) in (A.1), we can calculate the values of ω at which the height is half of the maximum height from the following equation

$$\mathrm{Im}\left[\frac{1}{\left[1 + \left(i\frac{1}{\tau_{max}}\right)^\alpha\right]^\beta}\right] = 2\,\mathrm{Im}\left[\frac{1}{[1 + (i\omega)^\alpha]^\beta}\right] \qquad (A.3)$$

which was numerically solved using Mathcad 13.0. Finally, with the two values of ω ($\omega_{+1/2}$ and $\omega_{-1/2}$) obtained from (A.3), we calculated the value of fwhm as

$$\mathrm{fwhm} = \log(\omega_{+1/2}) - \log(\omega_{-1/2}) \qquad (A.4)$$

We performed the calculations for several pairs of α and β, from 0.3 to 1. The obtained values of fwhm are shown in Figure 10 as a function of α and β.

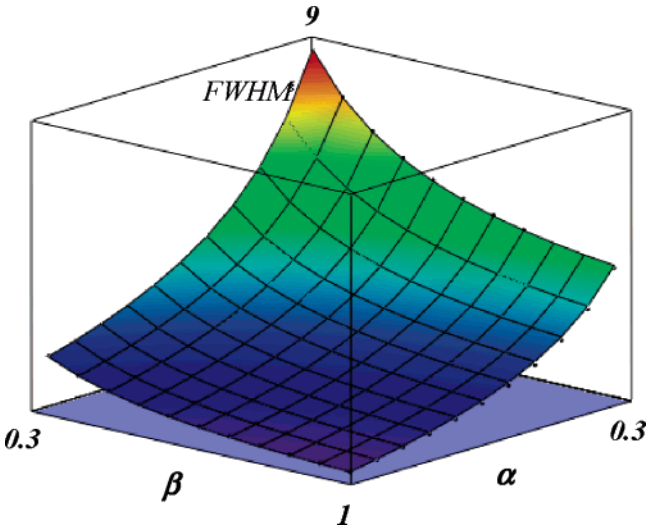

Figure 10. Numerically calculated values of fwhm as a function of α and β.

Now that we have numerically calculated the value of fwhm for several pairs of α and β, we will try to approximate fwhm by means of an empirical equation. After several attempts, we have found that the equation

$$\mathrm{fwhm}(\alpha,\beta) = -0.516 + \frac{1.058}{\alpha} + \frac{0.039}{\beta} + \frac{0.563}{\alpha\beta} \qquad (A.5)$$

gives an excellent description of the numerically obtained values of fwhm with an average precision better than 1%. Note that fwhm(1,1) = 1.144, which corresponds with the broadness of a Debye process.

References and Notes

(1) Chung, J. C.; Kornfield, J. A.; Smith, S. D. *Macromolecules* **1994**, *27*, 964.
(2) Lodge, T. P.; McLeish, T. C. B. *Macromolecules* **2000**, *33*, 5278.
(3) Alegría, A.; Colmenero, J.; Ngai, K. L.; Roland, C. M. *Macromolecules* **1994**, *27*, 4486.
(4) Wetton, R. E.; Macknight, W. J.; Fried, J. R.; Karasz, F. E. *Macromolecules* **1978**, *11*, 158. Shears, M. F.; Williams, G. *J. Chem. Soc., Faraday Trans. 2* **1973**, *4*, 608. Zetsche, A.; Fischer, E. W. *Acta Polym.* **1994**, *45*, 168.

(5) Lorthioir, C.; Alegría, A.; Colmenero, J. *Phys. Rev. E* **2003**, *68*, 031805.
(6) Genix, A. C.; Arbe, A.; Alvarez, F.; Colmenero, J.; Willner, L.; Richter, D. *Phys. Rev. E* **2005**, *72*, 031808.
(7) Tyagi, M.; Arbe, A.; Colmenero, J.; Frick, B.; Stewart, J. R. *Macromolecules* **2006**, *39*, 3007.
(8) Moreno, A. J.; Colmenero, J. *J. Chem. Phys.* **2006**, *124*, 184906.
(9) Corezzi, S.; Rolla, P. A.; Paluch, M.; Ziolo, J.; Fioretto, D. *Phys. Rev. E* **1999**, *60*, 4444.
(10) Casalini, R.; Capaccioli, S.; Lucchesi, M.; Rolla, P. A.; Corezzi, S. *Phys. Rev. E* **2001**, *63*, 031207. Prevosto, D.; Lucchesi, M.; Capaccioli, S.; Casalini, R.; Rolla, P. A. *Phys. Rev. B* **2003**, *67*, 174202.
(11) Roland, C. M.; Casalini, R. *Macromolecules* **2003**, *36*, 1361.
(12) Alegria, A.; Gomez, D.; Colmenero, J. *Macromolecules* **2002**, *35*, 2030.
(13) Schwartz, G. A.; Tellechea, E.; Colmenero, J.; Alegría, A. *J. Non-Cryst. Solids* **2005**, *351*, 2616.
(14) Schwartz, G. A.; Colmenero, J.; Alegría, A. *Macromolecules* **2006**, *39*, 3931.
(15) Floudas, G. In *Broadband Dielectric Spectroscopy*; Kremer, F., Schonhals, A., Eds.; Springer-Verlag: Berlin, 2003; Chapter 8.
(16) Mpoukouvalas, K.; Floudas, G.; Zhang, S. H.; Runt, J. *Macromolecules* **2005**, *38*, 552.
(17) Roland, C. M.; Casalini, R. *Macromolecules* **2005**, *38*, 8729.
(18) Roland, C. M.; McGrath, K. J.; Casalini, R. *Macromolecules* **2006**, *39*, 3581.
(19) Mpoukouvalas, K.; Floudas, G.; Zhang, S. H.; Runt, J. *Macromolecules* **2005**, *38*, 552.
(20) Cerveny, S.; Colmenero, J.; Alegria, A. *Macromolecules* **2005**, *38*, 7056.
(21) Schwartz, G. A.; Cangialosi, D.; Alegría, A.; Colmenero, J. *J. Chem. Phys.* **2006**, *124*, 154904.
(22) Pathak, J. A.; Colby, R. H.; Floudas, G.; Jerome, R. *Macromolecules* **1999**, *32*, 2553 and references therein.
(23) Cangialosi, D.; Schwartz, G. A.; Alegría, A.; Colmenero, J. *J. Chem. Phys.* **2005**, *123*, 144908.
(24) Floudas, G. In *Broadband Dielectric Spectroscopy*; Kremer, F., Schonhals, A. A., Eds.; Springer-Verlag: Berlin, 2003; Chapter 8.
(25) Takeno, H.; Kobayashi, M.; Aikawa, T. *Macromolecules* **2006**, *39*, 2183.
(26) Vogel, H. *Phys. Z.* **1921**, *22*, 645. Fulcher, G. S. *J. Am. Ceram. Soc.* **1923**, *8*, 339. Tammann, G.; Hesse, W. *Z. Anorg. Allg. Chem.* **1926**, *156*, 245.
(27) Casalani, R.; Roland, C. M. *Phys. Rev. E* **2004**, *69*, 062501.
(28) Alba-Simionesco, C.; Cailliaux, A.; Alegría, A.; Tarjus, G. *Europhys. Lett.* **2004**, *68*, 58.
(29) Roland, C. M.; Hensel-Bielowka, S.; Paluch, M.; Casalini, R. *Rep. Prog. Phys.* **2005**, *68*, 1405 and references therein.
(30) Sy, J. W.; Mijovic, J. *Macromolecules* **2000**, *33*, 933.
(31) Blochowicz, T.; Rössler, E. A. *Phys. Rev. Lett.* **2004**, *92*, 225701.
(32) Capaccioli, S.; Kessairi, K.; Prevosto, D.; Lucchesi, M.; Ngai, K. L. *J. Non-Cryst. Solids* **2006**, *352*, 4643.
(33) Corezzi, S.; Rolla, P. A.; Paluch, M.; Ziolo, J.; Fioretto, D. *Phys. Rev. E* **1999**, *60*, 4444.
(34) Naoki, M.; Endou, H.; Matsumoto, K. *J. Phys. Chem.* **1987**, *91*, 4169.
(35) Bendler, J. T.; Fontanella, J. J.; Shlesinger, M. F. *Phys. Rev. Lett.* **2001**, *87*, 195503.
(36) Roland, C. M.; Casalini, R.; Paluch, M. *Chem. Phys. Lett.* **2003**, *367*, 259.
(37) Ngai, K. L.; Casalini, R.; Capaccioli, S.; Paluch, M.; Roland, C. M. *J. Phys. Chem. B* **2005**, *109*, 17356.
(38) Roland, C. M.; Ngai, K. L. *Macromolecules* **1992**, *25*, 5765.
(39) Huang, D.; Colucci, D. M.; McKenna, G. B. *J. Chem. Phys.* **2002**, *116*, 3925.
(40) Mark, J. E. *Physical Properties of Polymers Handbook*; AIP Press: New York, 1996; Chapter 7.
(41) Zoller, P.; Walsh, D. *Standard Pressure-Volume-Temperature Data for Polymers*; Technomic Publishing Co.: Lancaster, PA, 1995; Chapter 13.

MA062609B